[Short title + Author Name - P&H title] 17 (2024) 105952

Contents lists available at ScienceDirect

Arabian Journal of Chemistry

journal homepage: www.ksu.edu.sa

Synthesized manganese oxide nanorods: Fabrication, characterization, application in cardiomyocyte protection from oxidative stress during sepsis, and evaluation of biochemical aspects of hemoglobin interaction

Jingjing Wang [a,1], Qianhu Liu [b,1], Wen Shi [c,1], Lulu Cao [d], Ruiming Deng [e], Teng Pan [f], Jinhai Deng [g], Zhenlan An [h,*], Shihui Fu [i], Teng Du [j,*], Chunxin Lv [a,*]

[a] Oncology Department, Shanghai Punan Hospital of Pudong New District, Shanghai, 200125, China
[b] General Practice Department, Shanghai Punan Hospital of Pudong New District, Shanghai, 200125, China
[c] Department of Dermatology, Shanghai Punan Hospital of Pudong New District, Shanghai, 200125, China
[d] Department of Rheumatology and Immunology, Peking University People's Hospital and Beijing Key Laboratory for Rheumatism Mechanism and Immune Diagnosis (BZ0135), Beijing, 100044, China
[e] Department of Anesthesiology, Ganzhou People's Hospital, Ganzhou, 341000,Jiangxi,China
[f] Longgang District Maternity & Child Healthcare Hospital of Shenzhen City (Longgang Maternity and Child Institute of Shantou University Medical College), Shenzhen, 518172, China
[g] Richard Dimbleby Department of Cancer Research, Comprehensive Cancer Centre, Kings College London, London, SE1 1UL, United Kingdom
[h] Intensive Care Unit, Shanghai Punan Hospital of Pudong New District, Shanghai, 200125, China
[i] Department of Cardiology, Chinese People's Hospital, Beijing, China
[j] Geriatric Department, Minhang Hospital, Fudan University, Shanghai, 201100, China

ARTICLE INFO

Keywords:
Magnesium oxide
Nanorods
Antioxidant
Interaction
Cardiac

ABSTRACT

Oxidative stress during sepsis could play a crucial role in the pathogenesis of several diseases, especially cardiovascular disorders. In fact, myocardial dysfunction during sepsis is caused by a number of chemicals, one of which is hydrogen peroxide (H_2O_2). Therefore, sepsis-induced cardiomyopathy can be controlled through modulation of oxidative stress. Despite the encouraging pharmacological activities demonstrated by inorganic nanostructures, the mechanisms behind their blood protein interaction and antioxidant activity remain unclear. In order to advance the investigation for fabricating nanostructure platforms and studying their antioxidant effects as well as blood protein binding affinities, we explored the synthesis of manganese oxide (Mn_3O_4) nanorods via hydrothermal method and subsequent characterization using various techniques. The antioxidant effects against H_2O_2-induced oxidative stress in AC16 cardiomyocytes were then evaluated by different cellular and molecular assays. Additionally, the interaction of Mn_3O_4 nanorods with hemoglobin was investigated by experimental and and docking analyses. The results showed that synthesized Mn_3O_4 nanorods had an absorption peak in the range of 260 to 420 nm, vibration bands centered at 510 cm^{-1}, 629 cm^{-1} and 410 cm^{-1}, 13 distinct XRD peaks, a rod-like morphology with a diameter range of 10 to 75 nm, a hydrodynamic size of 371.7 nm, and a zeta potential of −43.3 mV. Moreover, the antioxidant assays indicated that synthesized Mn_3O_4 nanorods can trigger a protective effect against H_2O_2-induced oxidative stress in AC16 cardiomyocytes through inhibition of reactive oxygen species (ROS) overproduction, increased content of superoxide dismutase (SOD) and catalase and glutathione (GSH), and reduction of caspase-3 activity. Furthermore, the fluorescence quenching mechanism of hemoglobin by Mn_3O_4 nanorods was determined to be controlled by a spontaneous and static quenching process, involvement of hydrogen bonds, a binding affinity (K_b) value of 10^4 M^{-1}, and number of binding site (n) of around 1.03. Additionally, it was found that Mn_3O_4 nanorods induced a slight conformational change in the hemoglobin structure, where Tyr35 and Trp37 move to a hydrophilic microenvironment. In conclusion, it can be suggested that Mn_3O_4 nanorods with a reasonable plasma protein binding affinity can be used as an antioxidant co-therapy in cardiac dysfunction during sepsis.

* Corresponding authors.
E-mail addresses: anzhen.lan@163.com (Z. An), yymc668@126.com (T. Du), lv_chunxin@fudan.edu.cn (C. Lv).
[1] The authors equally contributed to this work:Jingjing Wang, Qianhu Liu, Wen Shi.

https://doi.org/10.1016/j.arabjc.2024.105952
Received 30 August 2023; Accepted 5 August 2024
Available online 8 August 2024

1. Introduction

One of the leading causes of death in intensive care units is known to be sepsis. Even while the exact cause of sepsis is still unknown, there is growing confirmation that antioxidants and oxidants are important players (Mantzarlis et al., 2017). Reactive oxygen species (ROS) as one of the main metabolites generated by cells are typically produced in the mitochondrial electron transport chain and play a key role in intracellular signaling to mediate the normal physiological functions of cells (Brieger et al., 2012, Olajide et al., 2022). Typically, in normal conditions, the ROS generation and decomposition can be balanced through different enzymatic [superoxide dismutase (SOD), catalase (CAT), and glutathione reductase (GSH-Px)] and non-enzymatic antioxidant [reduced glutathione (GSH)] systems (Matés et al., 1999). However, upon generation of excessive levels of ROS, the cells may undergo physiological changes derived from oxidative stress (Brieger et al., 2012, Olajide et al., 2022). The production of high levels of ROS during sepsis is known as a main concern for the initiation and progression of several oxidative stress-associated disorders, including cardiovascular disease, cancers, neurodegenerative diseases, diabetes, and obesity (Essick and Sam 2010, Mantzarlis et al., 2017, Olajide et al., 2022, Cojocaru et al., 2023). In fact, oxidative stress during sepsis has been reported to play an important role in the development of several cardiovascular disorders, such as "heart failure, myocardial ischemia–reperfusion injury, and cardiomyopathy (Matés et al., 1999, Lakshmi et al., 2009, Mantzarlis et al., 2017, Zhang et al., 2018, Bertozzi et al., 2024). It has been reported that oxidative stress can trigger endothelial dysfunction in cardiovascular disorders (Shaito et al., 2022), pyroptosis and cardiac hypertrophy (Wang et al., 2022a), and proliferation of cardiac fibroblasts (Janbandhu et al., 2022).

An emerging field, nanotechnology has shown numerous potential applications in the sepsis diagnosis and management as well as the development of antioxidant platforms (Ghorbani et al., 2019, Roudbaneh et al., 2019, Pant et al., 2021, Fu et al., 2024). Nanoparticles are smaller than 100 nm in size and present a unique surface texture, size, shape, and chemical properties. Changing the physicochemical properties of materials at the nanoscale can cause magnetic, electrical, chemical, structural, and morphological changes, as well as associated protective effects. Therefore, nanomaterials with proper design can be used as potential antioxidant agents. Indeed, nanoparticles, particularly inorganic ones, show promising applications for the treatment of oxidative stress diseases via various signaling pathways (Ghorbani et al., 2019, Liu, Kim et al. 2021, Perez-Araluce et al., 2024).

One type of metal oxide nanoparticle that is commonly used in biomedical research as a potential antioxidant agent is manganese oxide (Mn_3O_4). For example, cerium oxide/Mn_3O_4 nanocrystals were used as potential antioxidants against acute radiation syndrome of stem cells (Han et al., 2020). Furthermore, a Mn_3O_4 nanozyme was able to prevent the oxidative stress and corresponding damage of biomolecules without a significant effect on the endogenous antioxidant system (Singh et al., 2019). Additionally, the redox capability of Mn_3O_4 nanostructures could be used as a potential strategy to alleviate the cytotoxicity in human cells (Singh et al., 2017).

Various methods have been used in the fabrication of Mn_3O_4 nanostructures for biomedical applications (Ding et al., 2020). In fact, the synthesis of Mn_3O_4 nanocrystals with different shapes such as nanoparticles, nanorods and nanofractals has been reported previously in different studies (Chen, Lai et al. 2006, Han et al., 2006). Depending on the desired property, nanorods with anisotropic shape can display special catalytic efficiency, plasmonic resonances, and biomedical properties. However, some well-established drawbacks such as reaction residuals and contaminations, toxicity, and aggregation in different biofluids may limit their biomedical applications. It appears that the hydrothermal method may result in the fabrication of nanorods based on well-controlled chemical reactions with minimal loss of (nano)materials, proper orientation of crystals, and the control of the size and surface of nanoparticles (Polsongkram et al., 2008).

Moreover, in recent years, the interactions between blood proteins and nanoparticles have received a great deal of attention in the scientific community. In fact, due to nanoparticles' ability to reach and interact with blood circulatory system, investigation of interactions between nanoparticles and blood macromolecules is essential. Hemoglobin as the main component of blood proteins, red blood cells, has a globular quaternary structure with four polypeptide chains as well as corresponding heme groups (Garabagiu 2011). It has shown that different nanoparticles had the potential to interact with hemoglobin with different binding affinities and induce some conformational changes on the protein structure. For example, it was shown that synthesized gold nanoparticles (25 nm) and hemoglobin are negatively charged at physiological pH and hydrophobic forces play a key role in the formation of the resultant complex (Garabagiu 2011). Li et al. also reported that upon the interaction of nanoparticles with different proteins, including hemoglobin, trypsin, lysozyme, pepsin, and γ-globulin, the protein concentration needed to result in the formation of stable protein corona is not comparable and the alterations in secondary conformer of protein is not directly correlated with the binding constant (Li et al., 2022).

As no direct study has been reported on the antioxidant and protein binding properties of Mn_3O_4 nanorods, in this study, we fabricated Mn_3O_4 nanorods using the hydrothermal method and after well-characterization using various techniques, their protective effects against sepsis-induced oxidative stress model in AC16 human cardiomyocytes as well as hemoglobin binding characteristics were investigated by different techniques.

2. Material and methods

2.1. Materials

Human hemoglobin (CAT Nr.: H7379), manganese (II) sulfate ($MnSO_4$, ≥99.99 % trace metals basis, CAT Nr: 229784), potassium permanganate ($KMnO_4$, ≥ACS reagent, ≥99.0 %, CAT Nr: 223468) were purchased from Sigma Aldrich (USA). All other chemicals used were of analytical grade.

2.2. Synthesis of Mn_3O_4 nanorods

Mn_3O_4 nanorods were prepared through the hydrothermal method as previously described with some modifications (El-Said et al., 2022). Briefly, $MnSO_4$ (1.69 g), $KMnO_4$ (3.1 g), and H_2O_2 (50 mL) were dissolved in deionized water (60 mL), followed by stirring for 60 min, transferring into the autoclave vessel (80 °C, 2 h). The samples were then washed with deionized water and ethanol and then dried in an oven at 80 °C (El-Said et al., 2022).

2.3. Characterization of synthesized Mn_3O_4 nanorods

The structural and colloidal features of synthesized Mn_3O_4 nanorods were determined through several analyses. Transmission electron microscopy (TEM) analysis was done at room temperature after drying a droplet of samples on the TEM grid. The image was then obtained using a JEOL 200CX at 80 kV. Dynamic light scattering (DLS) analysis was done at room temperature to determine the diameter and zeta potential value of synthesized Mn_3O_4 nanorods at aqueous using a Brookhaven Instrument. X-ray diffraction (XRD) analysis was done to determine the crystalline phase of fabricated Mn_3O_4 nanorods using a PANalytical X'Pert Pro with a Cu X-ray source (45 kV, 40 mA). UV–Vis spectrophotometry was used to determine the absorption characteristics of synthesized Mn_3O_4 NPs using a CARY 50–BIO UV–Vis spectrophotometer (Varian, Australia). FTIR analysis was also done on a Thermo scientific™ Nicolet iS™50 FTIR Spectrometer.

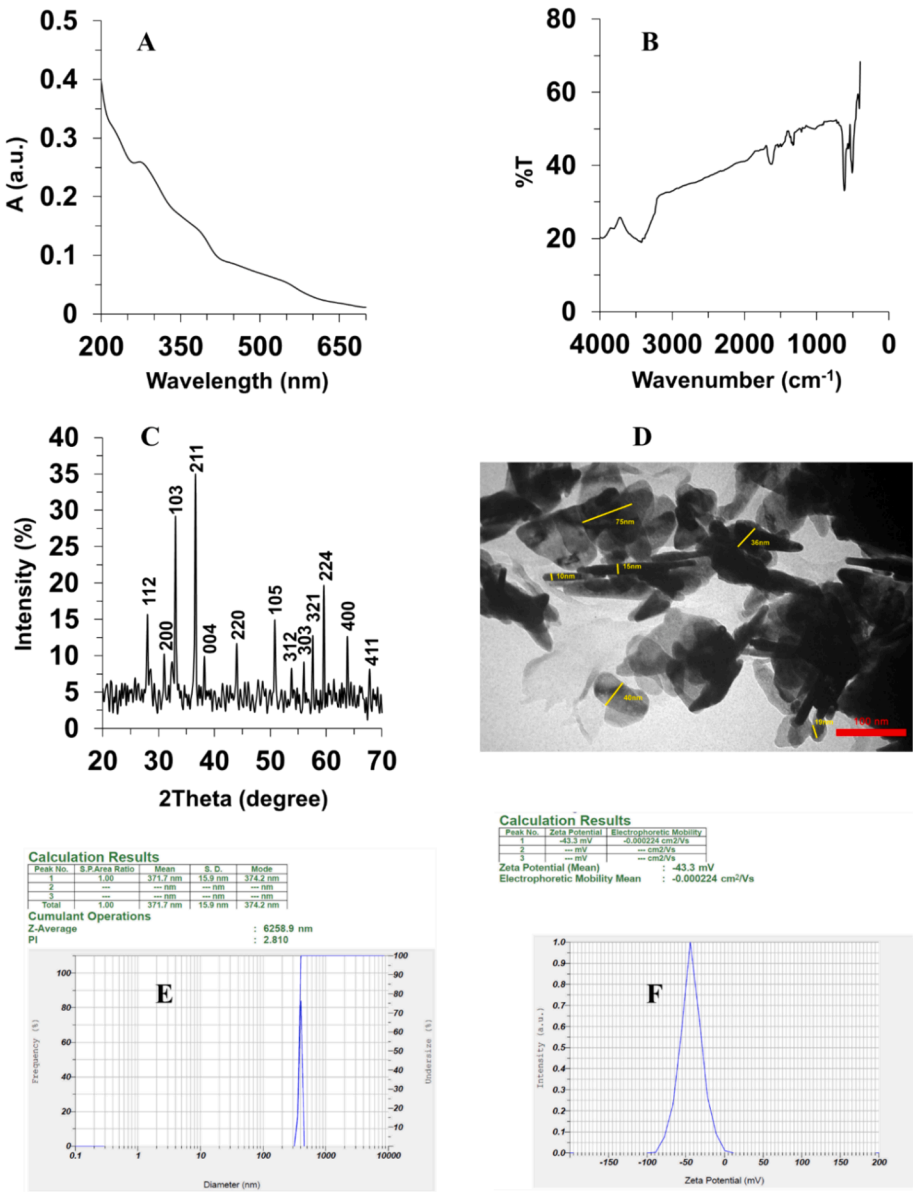

Fig. 1. Characterization of Mn_3O_4 nanorods through the hydrothermal method. (A) UV–vis spectroscopy, (B) Fourier transform-infrared spectroscopy (FTIR), (C) X-ray diffraction (XRD), (D) TEM analysis, (E) Zeta-sizer analysis for hydrodynamic size determination, (F) Zeta-sizer analysis for zeta potential determination.

2.4. Preparation of solutions

Mn_3O_4 nanorods were first exposed to UV for 50 min and then suspended in cell culture medium or phosphate-buffered saline (PBS; 0.9 % NaCl in 10 mM sodium phosphate buffer, pH 7.4) followed by sonication (30 min at 50 W) for cell culture or protein binding assays, respectively. Hemoglobin solution was also prepared in PBS (0.9 % NaCl in 10 mM sodium phosphate buffer, pH 7.4).

2.5. Cell culture

AC16 human cardiomyocyte cells were used to explore the antioxidant activity of Mn_3O_4 nanorods. AC16 cells obtained from American Type Culture Collection (ATCC, Virginia 20110–2209, USA) were cultured in Dulbecco's Modified Eagle Medium (DMEM) (Sigma, St. Louis, MO, USA) supplemented with 10 % fetal bovine serum (FBS) (Sigma, St. Louis, MO, USA) and 1 % penicillin–streptomycin solution at 37 °C and 5 % CO_2.

2.6. Oxidative stress model stimulated by H_2O_2

After culturing the cells, sepsis-induced oxidative stress model was performed by incubating AC16 cells with a fixed concentration of H_2O_2 (0.5 mM) for 6 h. AC16 cells without any H_2O_2 addition were considered as a control group.

2.7. Cell viability assay

The MTT assay was performed to assess the influence of H_2O_2 and Mn_3O_4 nanorods on the viability of AC16 cells. In the nanorod-related analyses, cells were incubated with increasing concentrations of Mn_3O_4 nanorods (0.1–50.0 μg/mL) for 24 h. In protective assays, AC16 cells were pretreated with Mn_3O_4 nanorods in a fixed concentration of 5 μg/mL (the maximum concentration of Mn_3O_4 nanorods with no significant cytotoxicity) for 18 h, followed by addition with 0.5 mM H_2O_2 for additional 6 h. Cells without any treatment were used as a control group. The cells were then added with MTT (5.0 mg/mL) for 4 h followed by replacing the medium with DMSO (150 μL) for 10 min. Finally,

the absorbance of samples was read at 570 nm on a microplate reader (Multiskan™ GO, Thermo Scientific, Waltham, MA, USA).

2.8. ROS assay

Intracellular ROS levels in AC16 cells (1×10^4 cells/well, 96-well plate) were assessed using 2',7'-dichlorofluorescein diacetate (DCF-DA) detection kit (Sigma-Aldrich, USA) based on the manufacturer's protocols. Briefly, after pretreating the cells with Mn_3O_4 nanorods with a concentration of 5 μg/mL for 18 h and further incubation with 0.5 mM H_2O_2 for 6 h, the cells were added by 0.3 mL of DCFH-DA probe for 30 min. Afterward, the cells were exposed to washing at least two times with DMEM. The fluorescence intensity was then measured using a fluorometer (Invitrogen, Carlsbad, CA, USA) at 485Ex/535Em nm.

2.9. ELISA assay for measuring the content of SOD, CAT and GSH

AC16 cells were seeded (1×10^6 cells/well in a 6-well plate) and treated. Then, the cells were lysed using RIPA lysis solution, and the levels of antioxidant enzymes [SOD (Catalog number: A001-1) and CAT (Catalog number: A007-2)], and non-enzymatic antioxidant [GSH (Catalog number: A006-1)] in AC16 cells were determined based on the protocols of assay kits (Nanjing Jiancheng Bioengineering Research Institute, Jiangsu, China).

2.10. Caspase-3 activity assay

The activity of caspase-3 was assessed using a Caspase-3 Activity Detection Kit (Beyotime Institute of Biotechnology, Shanghai, China). Briefly, 40 μL of the cells (1×10^4 cells/well in a 96-well plate) lysed using RIPA lysis solution lysates were added by 10 μL Ac-DEVD-PNA (2 mM) and incubated for 60 min. Finally, the activity of caspase-3 was determined at 570 nm on a microplate reader (Multiskan™ GO, Thermo Scientific, Waltham, MA, USA).

2.11. Fluorescence spectra

All fluorescence studies were performed on the F-7000 spectrofluorometer (Hitachi, Japan) employing a quartz cuvette of 1 cm path length. The excitation wavelength was fixed at 280 nm and the fluorescence spectra of hemoglobin (3 μM) either alone or with different concentrations of Mn_3O_4 nanorods (1–30 μM) was read in the wavelength range of 310–410 nm with a scan speed of 600 nm/min. The fluorescence experiments were done at 298 K, 305 K, and 310 K.

2.12. Circular dichroism (CD) studies

CD spectra of hemoglobin (3 μM) either alone or with a fixed concentration of Mn_3O_4 nanorods (30 μM) were read on JASCO J1500 CD spectrometer with a quartz cuvette of 1 mm path length. The wavelength range was set at 190–250 nm and the scan speed was fixed at 100 nm/min. All CD spectra were read at 298 K under continuous nitrogen flow.

2.13. Molecular docking study

A cylindrical (rod) Mn_3O_4 cluster with a 1 nm diameter and 4 nm length as well as a spherical Mn_3O_4 cluster with a dimension of 2 nm were constructed in Materials Studio software via repetition of the Mn_3O_4 oxide unit cell. All other Mn_3O_4 clusters were derived from cylindrical Mn_3O_4 clusters. The X-ray crystallographic 3D structure of human normal adult hemoglobin (PDB ID: 2H35) was downloaded from the online Protein Data Bank RCSB PDB (https://www.pdb.org). The docking simulations were performed on AutoDock Vina software. The docking box was centered on the protein structure and set to 80 x 70 x 80 Å with a spacing of 1 Å between grid points. The exhaustiveness parameter was set to 8 to ensure that the docking simulations were thorough. The binding energy and interaction forces were analyzed using Discovery Studio.

2.14. Statistical analysis

All assays in this study were done in triplicates and data were expressed as the mean ± standard deviation (SD) and the outcomes were analyzed by Student's *t*-test. The data were considered to be statistically significant at $P \leq 0.05$.

3. Results and discussion

3.1. Characterization of Mn_3O_4 nanorods

As a result of the importance of metal oxide nanoparticles in the development of potential antioxidant platforms and evaluation of their pharmacokinetic properties, the current report attempted to explore the characterization and antioxidant/protein binding properties of Mn_3O_4 nanorods prepared by hydrothermal method.

The absorption spectrum of Mn_3O_4 nanorods was analyzed using a UV–Vis spectrometer, in order to reveal their optical characteristics. In Fig. 1**A** the UV–Vis spectrum of Mn_3O_4 nanorods showed an absorption peak in the range of 260 to 420 nm deriving from charge transferrin between O^{2-}, Mn^{2+} and Mn^{3+} species (Vázquez-Olmos et al., 2005, Ghosh et al., 2017). Also, another absorption peak ranging from 420 nm to 700 nm can be associated with the d–d crystal field transitions observed on octahedral Mn^{3+} species (Vázquez-Olmos et al., 2005, Giri et al., 2014, Ghosh et al., 2017).

The FTIR spectrum of Mn_3O_4 nanorods is shown in Fig. 1**B**. The successful synthesis of Mn_3O_4 nanorods was further supported by the bands presented in the range of 410 cm^{-1} to 621 cm^{-1}. The Mn–O bond shows one stretching mode at around 621 cm^{-1} in a tetrahedral environment and one distortion vibration at around 510 cm^{-1} in an octahedral environment (Xing et al., 2011, Ghosh et al., 2017, Wang et al., 2021). Indeed, the peaks centered at around 510 cm^{-1}, 629 cm^{-1} and 410 cm^{-1} can be characteristics of the vibration of manganese species (Mn_3^+) in an octahedral state (Ghosh et al., 2017, Wang et al., 2021). Moreover, the characteristic bands at around 3420 and 1619 cm^{-1} were attributed to the hydroxyl groups (Shaik et al., 2021). These FTIR spectrum-based results are reliable with the data achieved from UV–vis characterization outcomes.

Furthermore, the crystallinity of Mn_3O_4 nanorods produced via hydrothermal method was assessed using XRD techniques as presented in Fig. 1**C**. XRD analysis indicated the presence of 13 distinct peaks attributed to 112, 200, 103, 211, 004, 220, 105, 312, 303, 321, 224, 400, and 411 crystalline phases (Fig. 1**C**), which is consistent with XRD values reported for Mn_3O_4 NPs (JCPDS No.24–0734) and previous studies (Shaik et al., 2021, Yewale et al., 2022).

Additionally, a TEM investigation was done to determine the shape and diameter of prepared Mn_3O_4 nanorods. The synthesized particles, as depicted in Fig. 1**D**, had a rod-like morphology and a diameter range of 10 to 75 nm. In general, it was realized that the size of synthesized nanorods was less than 80 nm. A variation in length was also found from 50 nm to greater amounts among the synthesized nanorods.

Furthermore, DLS analysis was used to determine the hydrodynamic radius of Mn_3O_4 nanorods, which revealed that the hydrodynamic size of prepared nanorods was 371.7 nm (Fig. 1**E**). According to the data, synthesized Mn_3O_4 nanorods may exhibit an agglomeration tendency in aqueous media. However, zeta potential analysis demonstrated that the charge distribution of fabricated Mn_3O_4 nanorods was about −43.3 mV (Fig. 1**F**), indicating the presence of a high surface charge to stabilize the nanoparticles against agglomeration (Yang et al., 2018). Therefore, it can be suggested that the prepared nanorods have good colloidal stability and dispersion properties.

In addition, Yang et al. reported the synthesis of Mn_3O_4 in the form of nanoparticles via laser ablation method and indicated the presence of

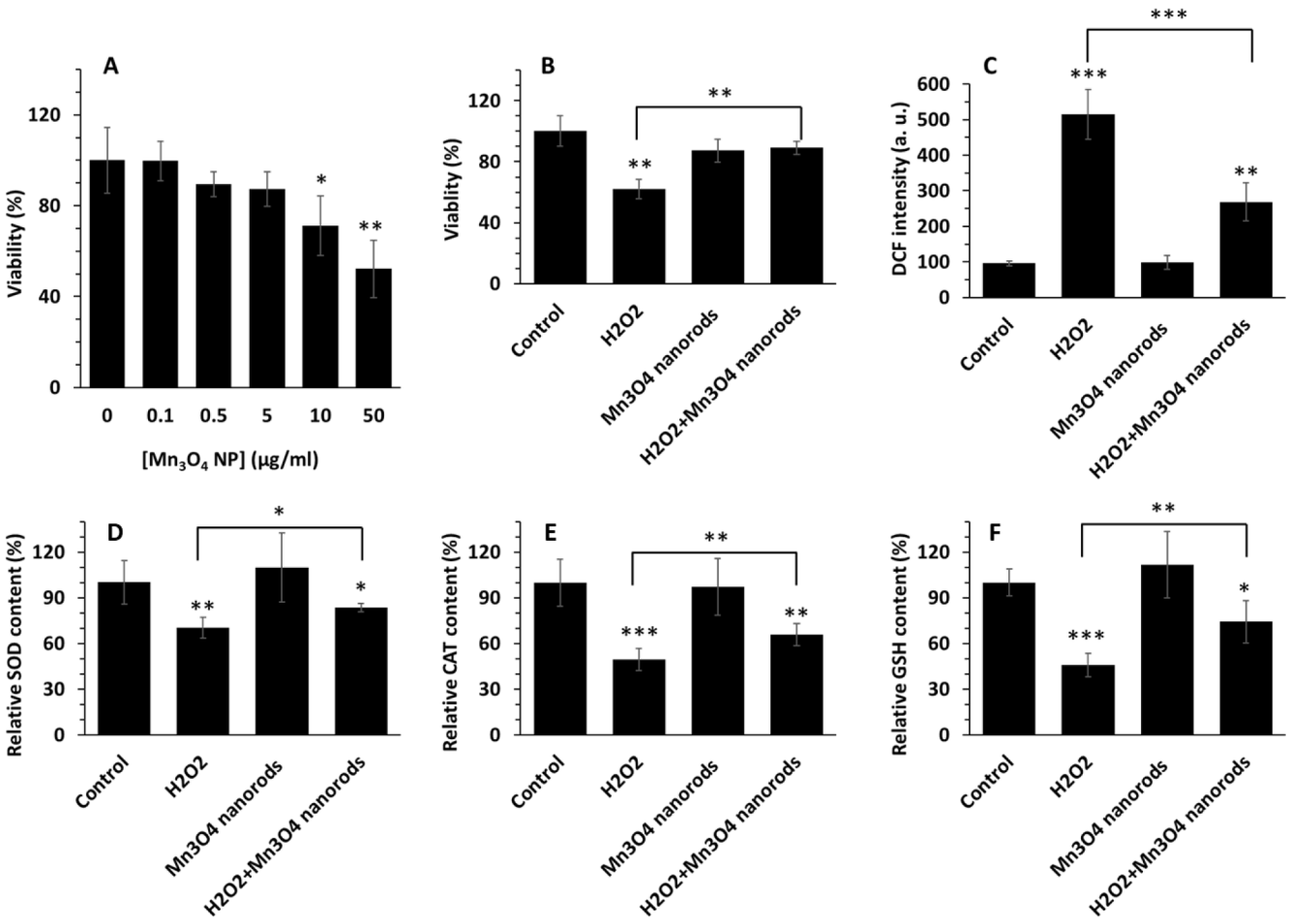

Fig. 2. AC16 cell viability in the presence of varying concentrations of Mn_3O_4 nanorods (0.1–50 µg/mL) after 24 h, evidenced by MTT assay (A). Protective effects of Mn_3O_4 nanorods (5 µg/mL) against H_2O_2 (0.5 mM)- induced cytotoxicity in AC16 cells, measured by MTT assay (B). Cells were pretreated with Mn_3O_4 nanorods (5 µg/mL) for 18 h and then added by H_2O_2 (0.5 mM) for additional 6 h. ROS assay for determination of oxidative stress induced by H_2O_2 (0.5 mM) and the protective effects of Mn_3O_4 nanorods pretreatment, assessed by DCF fluorescence intensity measurement (C). The contents of SOD (D), CAT (E), and GSH content (F) in AC16 cells treated with different samples, analyzed by ELISA assay. *$p < 0.5$, **$p < 0.01$, ***$p < 0.001$.

large coercivity and exchange bias in the structure of synthesized NPs (Yang et al., 2019). Furthermore, El-Said et al. reported that the hydrothermal-based synthesis of Mn_3O_4 nanorods with an average diameter of 100 ± 30 nm, evidenced by SEM imaging (El-Said et al., 2022), which is almost comparable with our TEM data. However, the authors did not report any DLS data to enable us to compare the hydrodynamic radius of prepared nanorods.

3.2. Effects of Mn_3O_4 nanorods on the viability of AC16 cells

In order to choose a suitable and safe concentration of Mn_3O_4 nanorods for protective effects against oxidative damage in AC16 cells, the cell viability was assessed by a well-known MTT assay. As displayed in Fig. 2**A**, the cell viability significantly declined when treated with Mn_3O_4 nanorods at concentrations of 10 and 50 µg/mL in comparison with the control group. Whereas, no significant differences in AC16 cell viability were detected in the range of 0.1 to 5 µg/mL of Mn_3O_4 nanorod treatments. Therefore, 5 µg/mL of Mn_3O_4 nanorods was determined as the appropriate concentration for inducing protective effects against sepsis-induced oxidative damage model *in vitro* in this study.

3.3. Effects of Mn_3O_4 nanorods on H_2O_2-triggered AC16 cytotoxicity

H_2O_2 has been widely used to induce oxidative damage during sepsis *in vitro* (Ben Saad et al., 2019). Hence, in this study, H_2O_2 was used to trigger sepsis-induced oxidative stress model in AC16 cells, *in vitro*. Then, the protective effect of Mn_3O_4 nanorods on H_2O_2 (0.5 mM)-stimulated cytotoxicity and oxidative stress in AC16 cells were assessed by cell viability and DCF assays. As exhibited in Fig. 2**B**, in comparison with the control, the incubation of the cells with 0.5 mM H_2O_2 for 6 h significantly (***$p < 0.001$) mitigated the cell viability to 62.16 ± 6.47 %, while pretreatment with Mn_3O_4 nanorods for 24 h revealed a significant recovery (**$p < 0.01$) in the cell viability compared to the H_2O_2 group, indicating that Mn_3O_4 nanorods may potentially prevent cytotoxicity in AC16 cells. Indeed, in the H_2O_2/ Mn_3O_4 nanorods treated group, the cell viability was calculated to be 89.10 ± 4.29 %, which was about 1.43- folds higher than the H_2O_2 group (**$p<0.01$). This data might be attributed to the promising antioxidant activity of Mn_3O_4 nanorods during sepsis, which was well-supported by the outcome of Singh et al. (Singh et al., 2019) and Adhikari et al. (Adhikari et al., 2017).

3.4. Effects of Mn_3O_4 nanorods on the generation of intracellular ROS

The incubation of Ac16 cells with H_2O_2can result in stimulation of the generation of excessive ROS during sepsis. At normal conditions due to low activity of antioxidant enzymes in AC16 cells, the ROS generated inside the cells can attack the intracellular components and lead to oxidative stress/damage during sepsis. ROS, a crucial indicator of oxidative stress, is closely associated with heart disorders (Takano et al.,

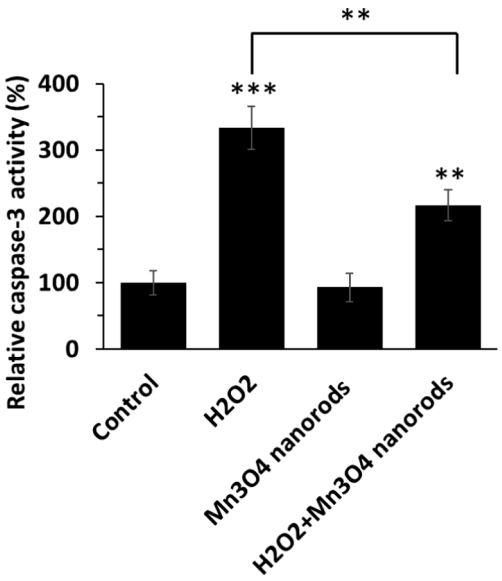

Fig. 3. Caspase-3 activity assay in AC16 cell treated with H_2O_2 (0.5 mM) for 6 h, Mn_3O_4 nanorods for 24 h, or pretreated with Mn_3O_4 nanorods (5 μg/mL) for 18 h and then added by H_2O_2 (0.5 mM) for additional 6 h. **p < 0.01, ***p < 0.001.

2003, Lin et al. 2013). Fig. 2**C** demonstrates the effects of Mn_3O_4 nanorods on ROS production of AC16 cells in response to H_2O_2-triggered oxidative stress. The level of ROS was significantly elevated in H_2O_2-treated cells (***p < 0.001), which were 5.38-fold higher compared to the control group. A probable suggestion for this phenomenon is that the addition of H_2O_2causes an oxygen reaction in the cells, leading to producing excessive amounts of ROS (Yoon et al., 2019). Whereas Mn_3O_4 nanorods pretreatment apparently (**p < 0.01) inhibited H_2O_2-triggered elevation of ROS level (Fig. 2**C**). These outcomes proposed that Mn_3O_4 nanorods played a protective effect in H_2O_2-induced AC16 cells by reducing the generation of ROS.

3.5. *Effects of Mn_3O_4 nanorods on the levels of SOD, CAT and GSH*

SOD, CAT, and GSH, crucial free radical scavengers, play a key role in inhibiting oxidative damage during sepsis (He, He et al. 2017, Kumar et al., 2018, Keshani et al., 2024). Importantly, SOD and CAT as antioxidant enzymes and GSH as a non-enzymatic antioxidant biomolecule can serve as free radical scavengers (Irato and Santovito 2021). Therefore, evaluating the levels of these biomolecules can be used as a potential indicator for determining the antioxidant activities of Mn_3O_4 nanorods. In this study, the influences of Mn_3O_4 nanorods on the levels of SOD, CAT and GSH in H_2O_2-triggered AC16 cells were assessed. As depicted in Fig. 2**D**, the SOD activity was significantly (*p < 0.05) declined in H_2O_2-triggered AC16 cells in comparison with the control cells, however promisingly increased in Mn_3O_4 nanorods-pretreated groups. The content of SOD was 83.52 ± 2.84 % in the Mn_3O_4 nanorods-pretreated groups, which was significantly higher than the H_2O_2 group (*p < 0.05), while lower than the control group (*p < 0.05).

CAT activity was also determined to be increased significantly in the Mn_3O_4 nanorods-pretreated group relative to the H_2O_2 group (**p < 0.01) (Fig. 2**E**), which well-agreed with the SOD results (Fig. 2**D**).

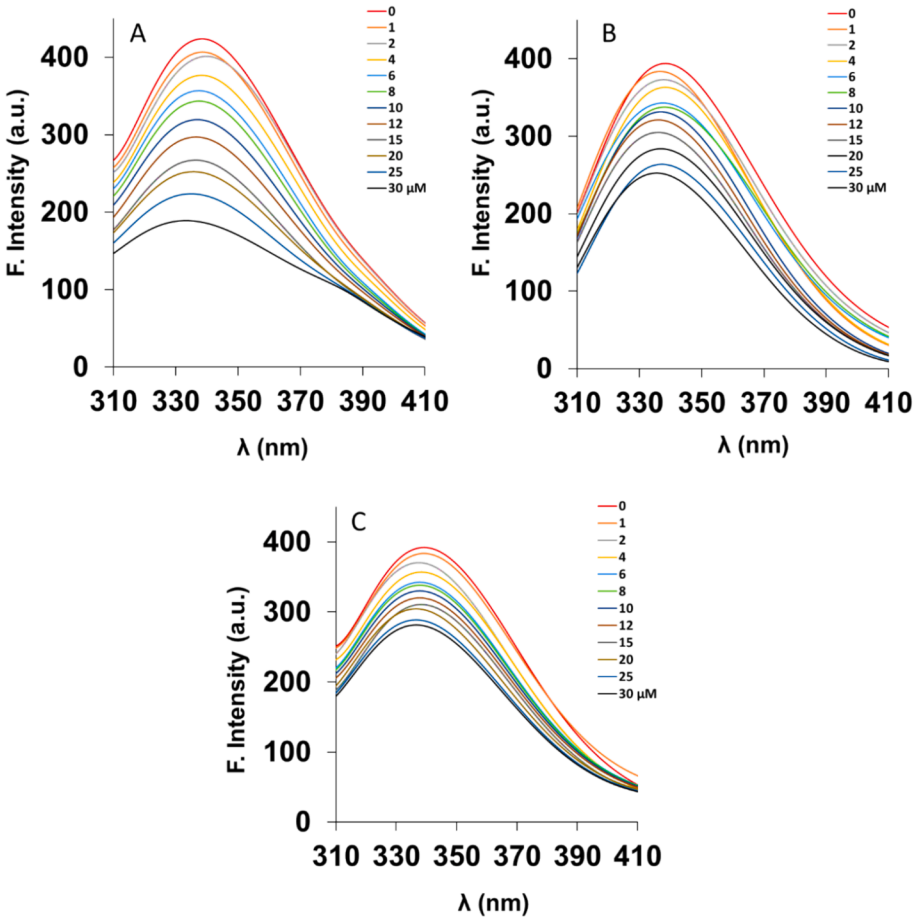

Fig. 4. Intrinsic fluorescence spectroscopy analysis of hemoglobin (3 μM) either alone or with different concentrations of Mn_3O_4 nanorods (1–30 μM) at 298 K (A), 305 K (B), and 310 K (C). The excitation wavelength was fixed at 280 nm.

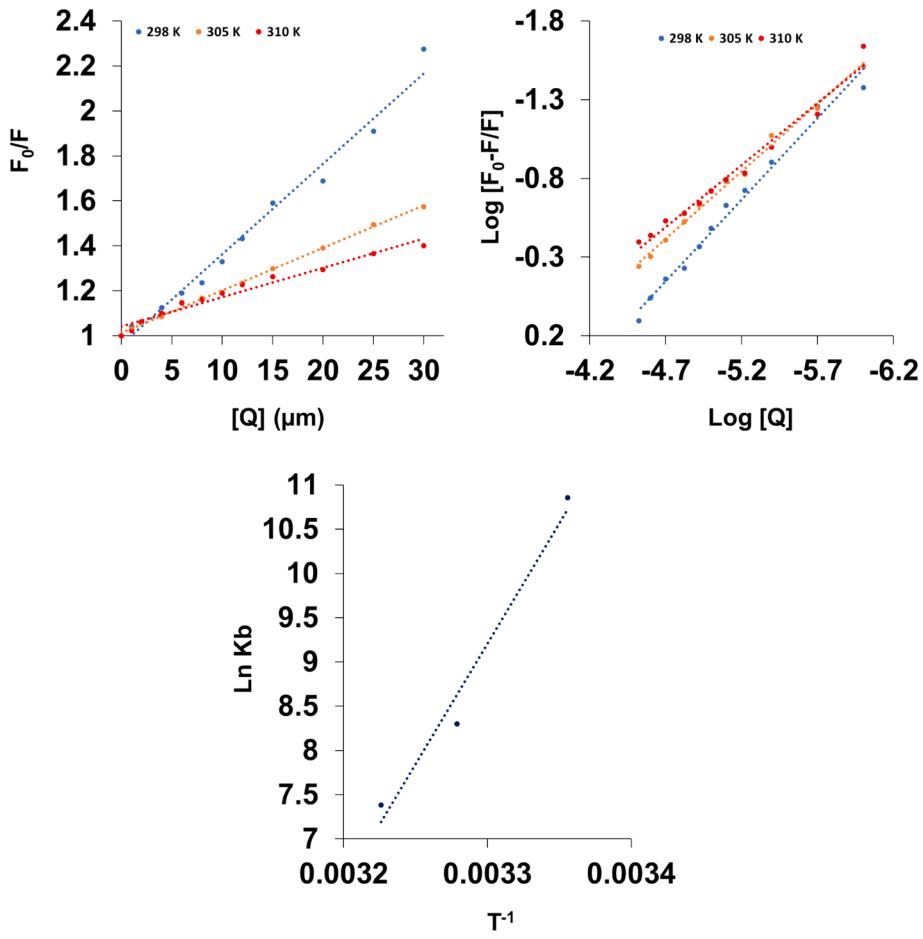

Fig. 5. Stern-Volmer (A), modified stern-Volmer (B) and van't Hoff (C) plots for the interaction of hemoglobin (3 μM) with different concentrations of Mn_3O_4 nanorods (1–30 μM).

In Fig. 2**F**, the GSH level was detected to have a 2.18-fold reduction in the H_2O_2 group in comparison with the control (***$p < 0.001$). After pretreatment with Mn_3O_4 nanorods, the level of GSH was enhanced, with a GSH level of 74.21 ± 13.81 %, significantly higher than that of the H_2O_2 group (45.73 ± 7.61 %) (**$p < 0.01$), which was the same as the SOD data.

In general, synthesized Mn_3O_4 nanorods showed potential antioxidant activity. Indeed, the aforementioned outcomes manifested that incubation with H_2O_2 could remarkably decrease the levels of SOD, CAT and GSH, while pretreatment with Mn_3O_4 nanorods could apparently recover the levels of these biomolecules in H_2O_2-stimulated cells as a model of oxidative stress during sepsis, indicating that Mn_3O_4 nanorods pretreatment may protect the cells against oxidative damage during sepsis through intensifying cellular antioxidant activity.

3.6. Caspase-3 activity

One common feature of cardiomyocyte oxidative damage during sepsis is apoptosis (Zhang et al., 2024). In fact, a number of studies indicate that ratio of Bax/Bcl-2, overexpressed by an excessive amount of ROS, induces the initiation of apoptosis by elevation of caspase-3 activity (Li et al. 2021, Fan et al., 2023). It has been shown that some modified nanoparticles can mitigate oxidative stress and apoptosis in myocardial cells during sepsis (Xiao and Chen 2020, Wang et al., 2022b). To further evaluate whether Mn_3O_4 nanorods are able to protect AC16 cardiomyocytes from H_2O_2-triggered apoptosis, we used a caspase-3 activity assay. As shown in Fig. 3, the activity of caspase-3 activity in the H_2O_2 group is markedly enhanced from 100 % to 333.12 ± 32.53 % in comparison with the control group, while Mn_3O_4 nanorods pretreatment reduced apoptosis induction on AC16 cells (216.56 ± 22.72 %). Indeed, Mn_3O_4 nanorods pretreatment led to a significant decrease in apoptosis rate (1.53-fold) compared to the H_2O_2 group (Fig. 3).

3.7. Mechanism of interaction of Mn_3O_4 nanorods with human hemoglobin

In the present study, we then analyzed the binding mode of the Mn_3O_4 nanorods to hemoglobin under simulated physiological conditions through intrinsic fluorescence measurements as well as CD study combined with molecular docking studies. Poor solubility of Mn_3O_4 nanorods in aqueous buffer solutions along with their heterogenous distribution disables the application of different types of calorimetry-based techniques for biomolecular interaction study. Then, we explored the consequences of Mn_3O_4 nanorod interaction and inspected their influence on the spatial and secondary structure of the protein by standard spectroscopic approaches. The purchased human hemoglobin was used to study the effects of prepared Mn_3O_4 nanorod on protein and we then compared our data with the literature, i.e., the binding affinity of the human hemoglobin–different nanoparticles.

3.7.1. Fluorescence quenching study

Quenching investigation of protein fluorescence induced by nanoparticles is known as a convenient approach for studying ligand-receptor interactions. The hemoglobin with a tetramer structure is composed of two αβ dimers. It has been shown that each dimer typically has three

Table 1
Quenching parameters of the interaction of Mn_3O_4 nanorods with hemoglobin at 298 K, 305 K, and 310 K.

T (K)	K_{SV} (M^{-1})	R^2	k_q (M^{-1} s^{-1})
298	4.02×10^4	0.98	4.02×10^{12}
305	1.89×10^4	0.99	1.89×10^{12}
310	1.30×10^4	0.96	1.30×10^{12}

Table 2
Binding parameters of the interaction of Mn_3O_4 nanorods with hemoglobin at 298 K, 305 K, and 310 K.

T (K)	$logK_b$	R^2	n
298	4.72	0.98	1.03
305	3.61	0.99	0.85
310	3.21	0.98	0.78

tryptophan (Trp) amino acid residues, namely α-Trp-14, β-Trp-15, and β-Trp-37. Moreover, five tyrosine (Tyr) amino acid residues are located in each αβ dimer: α-Tyr-24, α-Tyr-42, α-Tyr-140, β-Tyr-34, and β-Tyr-144 (Platanić Arizanović et al., 2023). Therefore, by excitation of the protein samples at 280 nm and the resultant changes in the intrinsic fluorescence of hemoglobin at 340 nm in the presence of the Mn_3O_4 nanorods may provide us with some useful detail regarding the local microenvironment of the Trp and Tyr moiety during binding (Cao et al., 2021, Li, Guo et al. 2022). Fig. 4 shows the typical quenching of hemoglobin fluorescence upon addition of increasing concentrations of the Mn_3O_4 nanorods. The optimum concentration of hemoglobin was fixed at 3 μM to reduce the auto-quenching of Trp/Tyr fluorescence by heme moieties (Hirsch and Nagel 1981, Platanić Arizanović et al., 2023). Human hemoglobin showed a strong fluorescence spectrum with a maximum emission at around 340 nm upon excitation at 280 nm, and Mn_3O_4 nanorods displayed a relatively low fluorescence intensity in comparison with the protein. Also, the probable fluorescence intensities of Mn_3O_4 nanorods were subtracted from the corresponding protein spectra. It was shown that Mn_3O_4 nanorods resulted in the fluorescence quenching of hemoglobin in a concentration-mediated manner at three temperatures of 298 K (Fig. 4**A**), 305 K (Fig. 4**B**), and 310 K (Fig. 4**C**), while no significant shift of the peak maximum was detected at all three temperatures. The data suggested that Mn_3O_4 nanorods interact with human hemoglobin and the fluorescence quenching could derive from a certain protein-nanorod complex formation (Li, Guo et al. 2022, Platanić Arizanović et al., 2023).

3.7.2. Quenching mechanism

The Stern-Volmer Eq. (1) was used to determine the quenching mechanism of human hemoglobin induced by Mn_3O_4 nanorods as follows (Platanić Arizanović et al., 2023):

$$F_0/F = 1 + k_q \times \tau_0[Q] = 1 + K_{SV} \times [Q] \quad (1)$$

where F_0 and F are receptor fluorescence at 340 nm without and with Mn_3O_4 nanorods, respectively, k_q defines the quenching rate constant, τ_0 is the average lifetime of the hemoglobin (10^{-8}), [Q] is the quencher (nanorod) concentration, and finally K_{SV} is the Stern-Volmer dynamic quenching constant, which can be determined from the slope of the linear F_0/F against [Q] plot. The Stern-Volmer plots of the human hemoglobin–Mn_3O_4 nanorod complex at different temperatures were shown to be almost linear for Mn_3O_4 nanorod concentrations up to 30 μM (Fig. 5**A**), suggesting that only one quenching mechanism (either static or dynamic) governs the protein quenching (Platanić Arizanović et al., 2023). In the static quenching mechanism, the formation of the ligand–protein system takes place in the ground state, while in the dynamic quenching mechanism the resultant complex is formed in the excited state of the fluorophore (van de Weert 2010). It was then deduced that K_{SV} values for the interaction of Mn_3O_4 nanorods and human hemoglobin were on the order of 10^4 M^{-1} (Table 1), revealing that there was a strong reduction in protein fluorescence with the addition of nanorods. Based on the data summarized in Table 1, the variations of the K_{SV} values are inversely proportional to temperature, characterizing the static quenching mechanism as a preferable process for the formation of Mn_3O_4 nanorods-hemoglobin complex (Ghalandari et al., 2022).

Also, the estimated values of k_q for the Mn_3O_4 nanorod binding to hemoglobin were found to be in the order of 10^{12} M^{-1} s^{-1} (Table 1), much greater than the reported value of 2×10^{10} M^{-1} s^{-1}, regarded as the basis of maximum associated constant in the dynamic quenching of macromolecules (Ware 1962). Therefore, this calculation further proved that the fluorescence quenching mechanism of hemoglobin is controlled by a static quenching process.

3.7.3. Binding affinity determination

When ligands/nanoparticles interact with proteins and attach independently to a set of equivalent sites on a receptor, the equilibrium between unbound and complex molecules is defined by the following Eq. (2) (Maity et al., 2017):

$$logF_0 - F/F = n \times log[Q] + \log K_b \quad (2)$$

where F_0 and F are the fluorescence intensities of protein without and with ligand (nanoparticle), [Q] is the concentration of ligand, n is the number of binding sites, and K_a is the binding constant. By plotting log (F_0 − F/F) against log [Q], the values of K_a and n can be evaluated. These parameters can characterize the binding affinity between a receptor and ligands/nanoparticles. Using Eq. (2) and the corresponding straight lines at three temperatures, the value of K_b and n for the binding of Mn_3O_4 nanorod with human hemoglobin were deduced from the intercept and slope of the double log plot, respectively (Fig. 5**B**). Following the inverse relationship between K_{SV} and temperature, K_b tends to decrease as temperature rises (Table 2).

It has been reported that ligands may bind reversibly with moderate affinity to proteins if the K_b value is in the magnitude of 10^4 M^{-1} (Dufour and Dangles 2005, Nedić et al., 2023, Platanić Arizanović et al., 2023). So, the K_b values determined in this study indicate that the binding between Mn_3O_4 nanorods and human hemoglobin was in the magnitude of 10^4 M^{-1} at 298 K and at higher temperatures, 305 K and 310 K, these values were reduced to the magnitude of 10^3 M^{-1}.

Therefore, it can be discussed that Mn_3O_4 nanorods show a moderate affinity to human hemoglobin and these nanoparticles can be stored and carried by this blood protein, used as a model, in the human body (Platanić Arizanović et al., 2023). In comparison with other nanoparticles, these binding constants were not comparable to those of the gold nanoparticles with a diameter of around 25 nm ($K_b = 1.893 \times 10^{10}$ M^{-1} at 301 K and $K_b = 22.715 \times 10^{10}$ M^{-1} at 311 K (Garabagiu 2011) and silver nanoparticles (5–10 nm) ($K_b = 1.30 \times 10^5$ at 310 K) (Zolghadri et al., 2009). However, it was found that the interaction of gold nanoparticles with a size of around 100 nm with hemoglobin results in the formation of a complex with K_b values of 1.4 to 2.2 $\times$ 10^5, depending on the temperature (Mandal et al., 2009). Also, upon the interaction of ferric oxide nanoparticles (10–20 nm) with human hemoglobin a K_b value of 6.10×10^4 was reported (Zolghadri et al., 2010). Therefore, it can be deduced that several parameters such as nanoparticle type, physicochemical properties of nanoparticles, and temperature can play a key role in the binding affinity of nanoparticles with proteins.

3.7.4. Thermodynamic study

The binding forces involved in the interactions of ligands with proteins mostly are van der Waals forces, hydrophobic effects, electrostatic interactions, and hydrogen bonding (Zeinabad et al., 2016). The thermodynamic parameters, [standard enthalpy change (ΔH°), standard entropy change (ΔS°), and standard Gibbs free energy change (ΔG°)] used as the main evidence for determining the binding forces between

Table 3
Thermodynamic parameters of the interaction of Mn_3O_4 nanorods with hemoglobin at 298 K, 305 K, and 310 K.

T (K)	ΔH° (kJ/mol)	ΔS° (J/mol.K)	ΔG° (kJ/mol)
298	−225.77	−668.56	−26.54
305			−21.86
310			−18.52

ligands and proteins are calculated from the van't Hoff Eq. (3) (Zeinabad et al., 2016):

$$\ln K_b = -\Delta H^\circ/R \times 1/T + \Delta S^\circ/R \quad (3)$$

and the Eq. (4):

$$\Delta G^\circ = \Delta H^\circ - T \times \Delta S^\circ \quad (4)$$

where K_b expresses the binding constant, R is the universal gas constant, and T denotes the absolute temperature. The values of ΔH° and ΔS° can

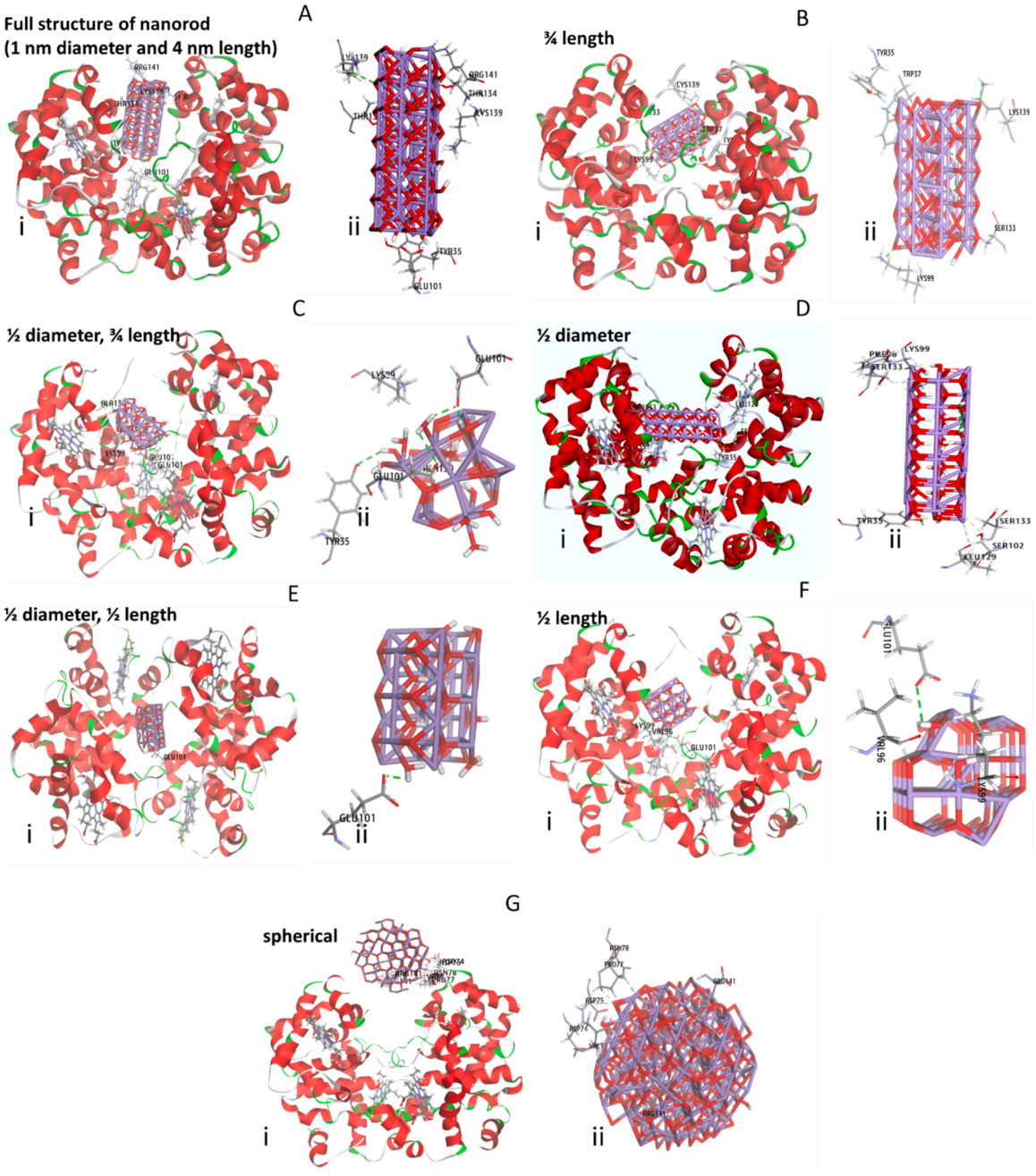

Fig. 6. Molecular docking study of the interaction of Mn_3O_4 clusters with hemoglobin. The interaction of Mn_3O_4 nanorods with a dimension of 1 nm diameter and 4 nm length and hemoglobin (i), amino acid residues in the binding pocket (ii) (A). The interaction of Mn_3O_4 nanorod with 3/4 length of original cluster and hemoglobin (i), amino acid residues in the binding pocket (ii) (B). The interaction of Mn_3O_4 nanorods with a dimension of ½ diameter, ¾ length of original cluster and hemoglobin (i), amino acid residues in the binding pocket (ii) (C). The interaction of Mn_3O_4 nanorod with a dimension of ½ diameter of original cluster and hemoglobin (i), amino acid residues in the binding pocket (ii) (D). The interaction of Mn_3O_4 nanorods with a dimension of ½ diameter, ½ length of original cluster and hemoglobin (i), amino acid residues in the binding pocket (ii) (E). The interaction of Mn_3O_4 nanorod with a dimension of ½ length of original cluster and hemoglobin (i), amino acid residues in the binding pocket (ii) (F). The interaction of Mn_3O_4 nanoparticles with a spherical shape and a size of 2 nm and hemoglobin (i), amino acid residues in the binding pocket (ii) (G).

Table 4
The interaction of Mn_3O_4 clusters (nanorods) with different geometries and human hemoglobin, studied by molecular docking analysis.

Type	Full structure of nanorod (1 nm diameter and 4 nm length)			
Interactions	**Distance**	**category**	**Type**	**Score (kcal/mol)**
C:LYS139:HN – ligand:O	2.81918	Hydrogen Bond	Conventional Hydrogen Bond	−15.41
A:LYS139:HE2 – ligand:O	2.14989	Hydrogen Bond	Carbon Hydrogen Bond	
A:LYS139:HE2 – ligand:O	2.511	Hydrogen Bond	Carbon Hydrogen Bond	
D:GLU101:OE1-ligand:MN –	2.25919	Other	Metal-Acceptor	
Type	¾ length			
A:LYS99:HZ3 – ligand:O	2.22402	Hydrogen Bond	Conventional Hydrogen Bond	−9.39
A:LYS139:HZ3 – ligand:O	2.71573	Hydrogen Bond	Conventional Hydrogen Bond	
D:TRP37:HE1 – ligand:O	2.6764	Hydrogen Bond	Conventional Hydrogen Bond	
A:SER133:OG – ligand:MN –	2.72698	Other	Metal-Acceptor	
Type	½ diameter, ¾ length			
B:GLU101:OE2 – ligand:H	1.29928	Hydrogen Bond	Conventional Hydrogen Bond	−4.18
D:GLU101:OE2 – ligand:H	2.71252	Hydrogen Bond	Conventional Hydrogen Bond	
B:GLU101:OE2 – ligand:H1	2.18796	Hydrogen Bond	Conventional Hydrogen Bond	
D:TYR35:OH – ligand:H	2.87338	Hydrogen Bond	Conventional Hydrogen Bond	
C:ALA130:O – ligand:H	2.83614	Hydrogen Bond	Conventional Hydrogen Bond	
Type	½ diameter			
B:TYR35:HH – ligand:O	2.31725	Hydrogen Bond	Conventional Hydrogen Bond	−5.70
C:LYS99:HA – ligand:O	2.48242	Hydrogen Bond	Carbon Hydrogen Bond	
C:SER133:HB2 – ligand:O	2.38252	Hydrogen Bond	Carbon Hydrogen Bond	
A:SER102:OG-ligand:MN	3.39788	Other	Metal-Acceptor	
A:LEU129:O – ligand:MN	3.30877	Other	Metal-Acceptor	
Type	½ diameter, ½, length			
B:GLU101:OE2 – ligand:H1	2.11782	Hydrogen Bond	Conventional Hydrogen Bond	−1.13
Type	length ½			
D:GLU101:OE1 – ligand:H	3.00628	Hydrogen Bond	Conventional Hydrogen Bond	−4.79
A:VAL96:HA – ligand:O	2.49543	Hydrogen Bond	Carbon Hydrogen Bond	
A:LYS99:HE1 – ligand:O	2.81764	Hydrogen Bond	Carbon Hydrogen Bond	
Type	Spherical			
C:ASN78:HD22 – ligand:O	1.68362	Hydrogen Bond	Conventional Hydrogen Bond	29.56
C:ASP75:HA – ligand:O	2.07268	Hydrogen Bond	Carbon Hydrogen Bond	
C:PRO77:HD1 – ligand:O	2.1597	Hydrogen Bond	Carbon Hydrogen Bond	

be calculated from the slope and intercept of the linear plot of $\ln K_a$ against 1/T under the assumption that these values are almost independent of absolute temperature (Platanić Arizanović et al., 2023). Also, protein does not experience significant structural changes at the studied temperatures (298 K, 305 K, and 310 K).

The sign of thermodynamic parameters contributed to receptor-ligand interaction provides useful information for the exploration of the discovery of binding forces involved between human hemoglobin and the nanoparticles tested. Therefore, the quenching analyses were performed at three different temperatures to ascertain the interaction thermodynamic factors. From the slope (ΔH°) and intercept (ΔS°) of the linear van't Hoff plots (ln K_a against 1/T; Fig. 5**C**) and Eqs. (3), (4), thermodynamic parameters were determined and summarized in Table 3.

In all temperatures, the negative value of the ΔG° reveals the spontaneity of the molecular interaction between Mn_3O_4 nanorods and hemoglobin (Zeinabad et al., 2016). The values of ΔH° (−225.77 kJ/mol) and ΔS° (−668.56 J/mol. K) were negative for Mn_3O_4 nanorods-hemoglobin system. The negative values of ΔH° and ΔS° apparently indicate that this complex formation is an enthalpy-driven and exothermic interaction mechanism (Zeinabad et al., 2016). Furthermore, the negative ΔS° value indicates that the randomness around the formed complex reduces (Zeinabad et al., 2016). The negative ΔS° value may suggest that hydrogen bonding is involved in the complexation of Mn_3O_4 nanorods with hemoglobin (Zeinabad et al., 2016). In fact, these findings were further verified by the molecular docking analysis (next sections).

3.8. Molecular docking study

Many studies have used molecular docking to examine the atomic-level interactions between ligands/nanoparticles and proteins. The findings gained from molecular docking analysis can be used to learn more about the interaction forces and the different ways that ligands and proteins bind. In this study, the interaction of Mn_3O_4 nanorods with human hemoglobin was studied by molecular docking analysis. As in the TEM investigation, a heterogenous distribution of Mn_3O_4 nanorods was observed, we tried to design different kinds of Mn_3O_4 clusters showing different dimensions and explore their interaction with hemoglobin. First of all, we designed a Mn_3O_4 nanorod with a dimension of 1 nm diameter and 4 nm length and explored its interaction with hemoglobin. As shown in Fig. 6**A**, Mn_3O_4 nanorods interact with the region between α/β subunits (Fig. 6**A**(i)), while Lys 139 and Glu 131 have surrounded this cluster (Fig. 6**A**(ii), Table 4). Also, it was shown that these amino acid residues are in a distance in the range of 2.14–2.81 with oxygen atoms of ligands and can result in the formation of conventional hydrogen bonds and carbon-hydrogen bonds. The latter forces are regarded as covalent, which may result in a strong binding energy between Mn_3O_4 nanorods and hemoglobin (−15.41 kcal/mol, Table 4). The contribution of Lys 139 in the formation of hydrogen bonds is in line with experimental thermodynamic parameters. To further analyze the interaction of Mn_3O_4 nanorods with hemoglobin, different types of nanoclusters were designed. Therefore, the interactions of Mn_3O_4 nanorods with 3/4 length (Fig. 6**B** (i, ii)), ½ diameter, ¾ length (Fig. 6**C** (i, ii)), ½ diameter (Fig. 6**D** (i, ii)), ½ diameter, ½ length (Fig. 6**E** (i, ii)), ½ length (Fig. 6**F** (i, ii)), as well as spherical Mn_3O_4 clusters (2 nm) (Fig. 6**G** (i, ii)) with hemoglobin were assessed and the resultant data were summarized in Table 4. As summarized in Table 4, it can be observed that Mn_3O_4 nanorods with 1 nm diameter and 4 nm length showed the strongest binding affinity (−15.41 kcal/mol) with hemoglobin among all other types of clusters, followed by Mn_3O_4 nanorods with ¾ length (−9.39 kcal/mol), ½ diameter (−5.70 kcal/mol), ½ length (−4.79 kcal. mol), ½ diameter, ¾ length ½ (−4.18 kcal/mol), ½ diameter, ½ length (−1.13 kcal/mol), and spherical shape (2 nm, 29.56 kcal/mol). Therefore, it may be discussed that although all designed clusters have the same chemical composition, their binding energies can vary. Additionally, it was found that for all clusters the main dominant force upon the interaction of Mn_3O_4 nanorods with human hemoglobin was hydrogen bonding, which is in good agreement with experimental outcomes. Also, based on fluorescence spectroscopy data which determined that fluorescence quenching occurs in the presence of varying concentrations of Mn_3O_4 nanorods, we can claim that Tyr35 (interaction of ½ diameter/¾ length and ½ diameter Mn_3O_4 clusters with hemoglobin) and Trp37 (interaction of ¾ length Mn_3O_4 cluster with hemoglobin) are placed in the vicinity of binding site of Mn_3O_4 clusters-hemoglobin complex.

Additionally, the solvent-accessible surface (SAS) of the ligand is

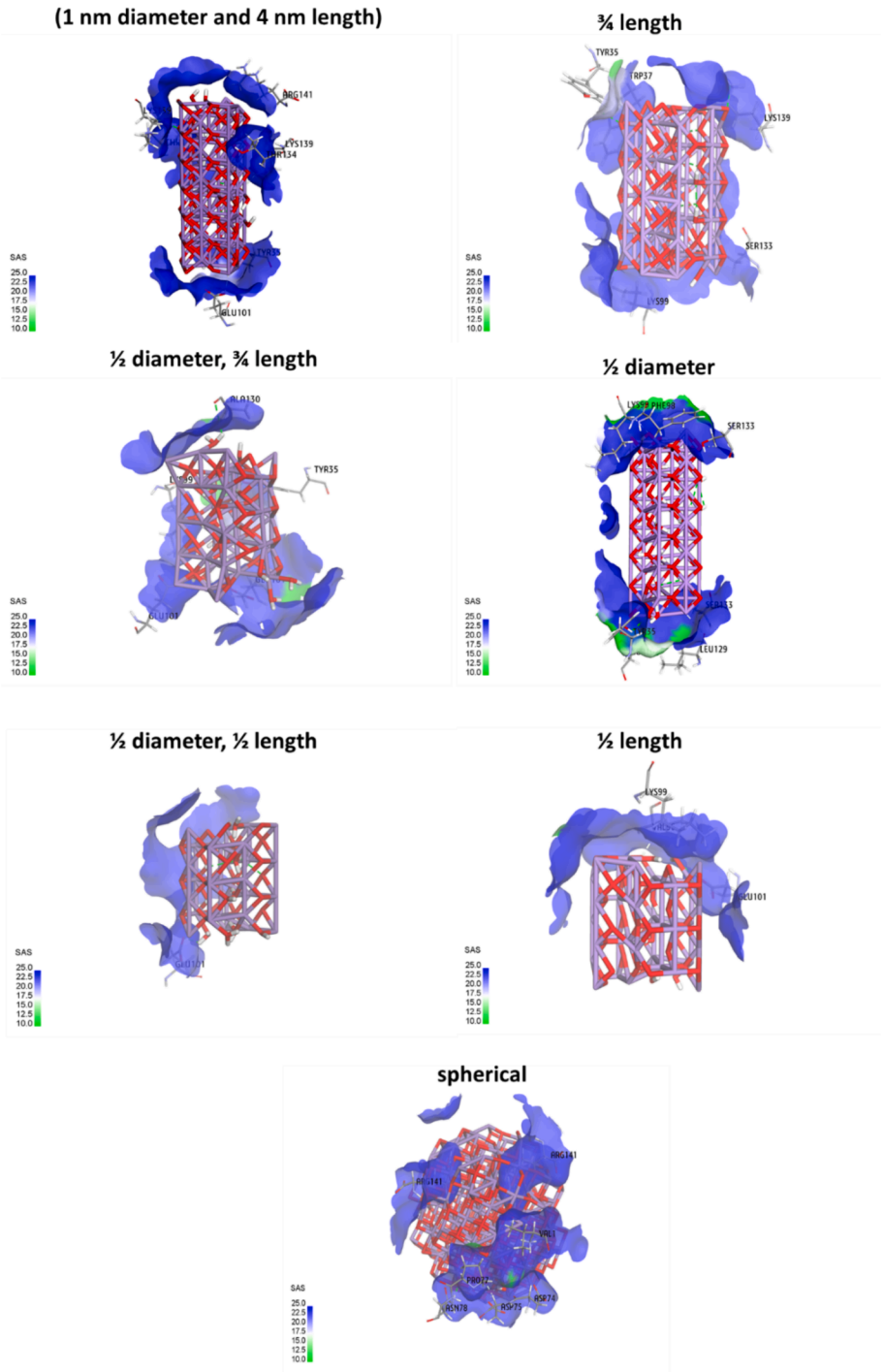

Fig. 7. Determination of solvent accessible surface (SAS) of Mn_3O_4 nanorod determined by molecular docking study of the interaction of Mn_3O_4 clusters with hemoglobin.

often less than that of the free ligand when it interacts with proteins because a portion of the ligand that was solvent accessible in the free forms is buried during interaction. As shown in Fig. 7, the surface area of designed clusters is heavily correlated with their morphology, as Mn_3O_4 clusters with 1 nm diameter and 4 nm length as well as ½ diameter exhibited the highest levels of ASA among the designed clusters. It reveals that these clusters have failed to reach the core site of hemoglobin and preferentially bind to the surface amino acid residues.

3.9. Circular dichroism study

To obtain a further understanding of secondary structural changes of the hemoglobin in the presence of Mn_3O_4 nanorods, a CD study was carried out. This technique is a quantitative and sensitive approach studying the structure of proteins in an aqueous solution (Zeinabad et al., 2016). From Fig. 8, an intensive positive peak at 195 nm and 2 negative minima at 208 and 222 nm were observed, characterizing the presence of α-helical structure (Chakraborty et al., 2018). Thus, a thorough understanding of the secondary structure of hemoglobin was gained from far-UV CD analysis in the wavelength range of 190 to 250

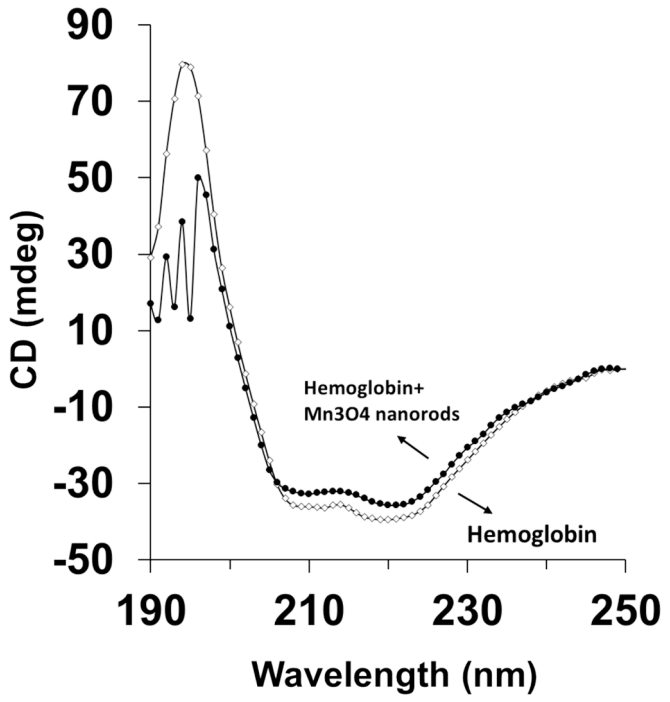

Fig. 8. Circular dichroism (CD) spectroscopy study of hemoglobin (3 μM) either alone or with Mn_3O_4 nanorods (30 μM) at 298 K.

nm. As shown in Fig. 8, the intensities of all bands at 195, 208 and 222 nm decrease upon the addition of Mn_3O_4 nanorods (30 μM). Indeed, in the presence of Mn_3O_4 nanorods (30 μM), the reduction in the ellipticity changes of the negative minima at 208 and 222 nm as well as the positive peak at 196 nm, provide us with some information regarding the secondary structural changes of hemoglobin in the presence of Mn_3O_4 nanorods. Quantitative analysis of the α-helix percentage in hemoglobin either alone or with Mn_3O_4 nanorods was determined by CDNN software. It was determined that the α-helix percentage of free hemoglobin was around ~ 61.24 %, while this amount decreased to ~ 58.77 % in the presence of Mn_3O_4 nanorods (30 μM). It has also been determined that gold nanoparticles after the interaction with hemoglobin resulted in a slight decrease in the α-helix percentage of protein (Chakraborty et al., 2018). In fact, the CD spectra of human hemoglobin at both minima, in the absence and presence of Mn_3O_4 nanorods altered slightly and seem to be comparable in shape. Thus, this observation revealed that the structure of hemoglobin remained predominantly α-helical even upon the interaction with the highest concentration of Mn_3O_4 nanorods (30 μM).

Furthermore, it has been shown that ferric oxide nanoparticles (10–20 nm) did not induce any alteration in the secondary structure of hemoglobin even up to 40 M, evidenced by CD analysis (Zolghadri et al., 2010). However, it was found that the addition of silver nanoparticles (5–10 nm) with different concentrations of 18.7, 37.4, and 74.8 μM to hemoglobin solution resulted in a significant change in the secondary structure of the protein (Zolghadri et al., 2009), while green synthesized hexagonal silver nanoparticle did not induce a significant effect (Shahabadi et al., 2023). Additionally, Chetty et al. reported that cerium oxide nanoparticles (20.9 nm) with different concentrations of 25 μM and 150 μM upon the interaction with Hb led to a significant decrease in minima at 222 and 211 nm with around 20 and 50 % reduction of α-helices, respectively (Chetty and Singh 2020). Therefore, upon addition of Mn_3O_4 nanorods, the spectral shape of hemoglobin remains almost unchanged though a marginal variation in the amount of ellipticity, CD signal, was detected. This data indicated that although slight alterations had appeared in the secondary structure of hemoglobin as anticipated for the interaction of (nano)particles, the overall secondary structure of the protein was normally unchanged and its integrity was kept intact even after the interaction with a high concentration of Mn_3O_4 nanorods. Therefore, after the interaction of Mn_3O_4 nanorods with blood proteins like hemoglobin, we can deduce that no significant change in the secondary structural pattern of the proteins may occur.

All these findings stipulated that Mn_3O_4 nanorods may be employed as a promising co-antioxidant therapy.

4. Conclusion

In conclusion, in the present study, nanorod-shaped Mn_3O_4 NRs synthesized through the hydrothermal method were shown to have a size of around 10–75 nm with good colloidal stability. Afterward, it was shown that synthesized Mn_3O_4 nanorods triggered antioxidant effects against H_2O_2-triggered oxidative stress, as a model of oxidative stress during sepsis, in AC16 cardiomyocyte cells through elevation of both enzymatic and non-enzymatic antioxidant systems. Furthermore, the study of direct interaction between Mn_3O_4 nanorods and hemoglobin showed that the synthesized nanoparticles form a static complex with protein through the contribution of hydrogen bonds. Moreover, it was shown that the secondary structure of hemoglobin underwent minor changes through reduction of α-helix percentage and displacement of Tyr35 as well as Tyr 37 amino acid residues.

Lastly, we should highlight the primary limitations of this study, which included the production of Mn_3O_4 nanorods using a single synthetic technique and the examination of a single signaling pathway/target for the assessment of the compounds' effects on protein binding and antioxidants. Antioxidant signaling pathways during sepsis triggered by Mn_3O_4 nanorods with varying physicochemical parameters need to be further studied in future studies employing both *in vitro* and *in vivo* testing. Also, protein binding properties of Mn_3O_4 nanorods with other blood proteins as well as protein corona formation should be investigated to provide us with detailed information about opsonization and direct interaction of nanoparticles with proteins.

CRediT authorship contribution statement

Jingjing Wang: Conceptualization, Methodology, Data analysis, Data verification, Writing the main manuscript, Software. **Qianhu Liu:** Conceptualization, Methodology, Data analysis, Data verification, Writing the main manuscript. **Wen Shi:** Conceptualization, Methodology, Data analysis, Writing the main manuscript. **Lulu Cao:** Conceptualization, Methodology, Writing the main manuscript. **Ruiming Deng:** Conceptualization, Methodology, Writing the main manuscript. **Teng Pan:** Conceptualization, Methodology, Data analysis. **Jinhai Deng:** Conceptualization, Methodology, Data analysis. **Zhenlan An:** Conceptualization, Supervision, Data analysis, Data verification, Writing the main manuscript, Software. **Shihui Fu:** Conceptualization, Writing the main manuscript. **Teng Du:** Conceptualization, Supervision, Data analysis, Data verification, Writing the main manuscript, Software. **Chunxin Lv:** Conceptualization, Supervision, Data analysis, Data verification, Writing the main manuscript, Software.

Declaration of competing interest

The authors declare that they have no known competing financial interests or personal relationships that could have appeared to influence the work reported in this paper.

Acknowledgements

This work has been reported in this study received no external funding.

References

Adhikari, A., Polley, N., Darbar, S., Pal, S.K., 2017. Therapeutic potential of surface functionalized Mn_3O_4 nanoparticles against chronic liver diseases in murine model. Materials Focus 6 (3), 280–289.

Ben Saad, H., Ben Amara, I., Kharrat, N., Giroux-Metges, M.-A., Hakim, A., Zeghal, K.M., Talarmin, H., 2019. Cytoprotective and antioxidant effects of the red alga Alsidium corallinum against hydrogen peroxide-induced toxicity in rat cardiomyocytes. Arch. Physiol. Biochem. 125 (1), 35–43.

Bertozzi, G., Ferrara, M., Di Fazio, A., Maiese, A., Delogu, G., Di Fazio, N., Tortorella, V., La Russa, R., Fineschi, V., 2024. Oxidative stress in sepsis: A focus on cardiac pathology. Int. J. Mol. Sci. 25 (5), 2912.

Brieger, K., Schiavone, S., Miller Jr, F.J., Krause, K.-H., 2012. Reactive oxygen species: from health to disease. Swiss Med. Wkly. 142 (3334), w13659–w.

Cao, L., Li, J., Song, Y., Cong, S., Wang, H., Tan, M., 2021. Molecular interaction of fluorescent carbon dots from mature vinegar with human hemoglobin: Insights from spectroscopy, thermodynamics and AFM. Int. J. Biol. Macromol. 167, 415–422.

Chakraborty, M., Paul, S., Mitra, I., Bardhan, M., Bose, M., Saha, A., Ganguly, T., 2018. To reveal the nature of interactions of human hemoglobin with gold nanoparticles having two different morphologies (sphere and star-shaped) by using various spectroscopic techniques. J. Photochem. Photobiol. B Biol. 178, 355–366.

Chen, Z.W., Lai, J.K.L., Shek, C.H., 2006. Shape-controlled synthesis and nanostructure evolution of single-crystal Mn_3O_4 nanocrystals. Scr. Mater. 55 (8), 735–738.

Chetty, R., Singh, M., 2020. In-vitro interaction of cerium oxide nanoparticles with hemoglobin, insulin, and dsDNA at 310.15 K: Physicochemical, spectroscopic and in-silico study. Int. J. Biol. Macromol. 156, 1022–1044.

Cojocaru, K.-A., Luchian, I., Goriuc, A., Antoci, L.-M., Ciobanu, C.-G., Popescu, R., Vlad, C.-E., Blaj, M., Foia, L.G., 2023. Mitochondrial dysfunction, oxidative stress, and therapeutic strategies in diabetes, obesity, and cardiovascular disease. Antioxidants 12 (3), 658.

Ding, B., Zheng, P., Ma, P.a., Lin, J., 2020. Manganese oxide nanomaterials: synthesis, properties, and theranostic applications. Adv. Mater. 32 (10), 1905823.

Dufour, C., Dangles, O., 2005. Flavonoid–serum albumin complexation: determination of binding constants and binding sites by fluorescence spectroscopy. Biochimica et Biophysica Acta (BBA)-General Subjects 1721 (1–3), 164–173.

El-Said, W.A., Alsulmi, A., Alshitari, W., 2022. Hydrothermal synthesis of Mn_3O_4 nanorods modified indium tin oxide electrode as an efficient nanocatalyst towards direct urea electrooxidation. PLoS One 17 (8), e0272586.

Essick, E.E., Sam, F., 2010. Oxidative stress and autophagy in cardiac disease, neurological disorders, aging and cancer. Oxid. Med. Cell. Longev. 3, 168–177.

Fan, M., Liang, T., Xie, F., Ma, P., Li, J., 2023. Exosomal circ_HIPK3 reduces apoptosis in H_2O_2-induced AC16 cardiomyocytes through miR-33a-5p/IRS1 axis. Transpl. Immunol. 101862.

Fu, J., Cai, W., Pan, S., Chen, L., Fang, X., Shang, Y., Xu, J., 2024. Developments and trends of nanotechnology application in sepsis: A comprehensive review based on knowledge visualization analysis. ACS Nano 18 (11), 7711–7738.

Garabagiu, S., 2011. A spectroscopic study on the interaction between gold nanoparticles and hemoglobin. Mater. Res. Bull. 46 (12), 2474–2477.

Ghalandari, B., Asadollahi, K., Ghorbani, F., Ghalehbaghi, S., Rafiee, S., Komeili, A., Kamrava, S.K., 2022. Determinants of gold nanoparticle interactions with Proteins: Off-Target effect study. Spectrochim. Acta A Mol. Biomol. Spectrosc. 269, 120736.

Ghorbani, M., Derakhshankhah, H., Jafari, S., Salatin, S., Dehghanian, M., Falahati, M., Ansari, A., 2019. Nanozyme antioxidants as emerging alternatives for natural antioxidants: Achievements and challenges in perspective. Nano Today 29, 100775.

Ghosh, S., Basu, S., Baskey, M., 2017. Decorating mechanism of Mn_3O_4 nanoparticles on reduced graphene oxide surface through reflux condensation method to improve photocatalytic performance. J. Mater. Sci. Mater. Electron. 28, 17860–17870.

Giri, A., Goswami, N., Sasmal, C., Polley, N., Majumdar, D., Sarkar, S., Bandyopadhyay, S.N., Singha, A., Pal, S.K., 2014. Unprecedented catalytic activity of Mn_3O_4 nanoparticles: potential lead of a sustainable therapeutic agent for hyperbilirubinemia. RSC Adv. 4 (10), 5075–5079.

Han, Y.-F., Chen, F., Zhong, Z., Ramesh, K., Chen, L., Widjaja, E., 2006. Controlled synthesis, characterization, and catalytic properties of Mn_2O_3 and Mn_3O_4 nanoparticles supported on mesoporous silica SBA-15. J. Phys. Chem. B 110 (48), 24450–24456.

Han, S.I., Lee, S.w., Cho, M.G., Yoo, J.M., Oh, M.H., Jeong, B., Kim, D., Park, O.K., Kim, J., Namkoong, E., 2020. Epitaxially strained CeO_2/Mn_3O_4 nanocrystals as an enhanced antioxidant for radioprotection. Adv. Mater. 32 (31), 2001566.

He, L., He, T., Farrar, S., Ji, L., Liu, T., Ma, X., 2017. Antioxidants maintain cellular redox homeostasis by elimination of reactive oxygen species. Cell. Physiol. Biochem. 44 (2), 532–553.

Hirsch, R.E., Nagel, R., 1981. Conformational studies of hemoglobins using intrinsic fluorescence measurements. J. Biol. Chem. 256 (3), 1080–1083.

Irato, P., Santovito, G., 2021. Enzymatic and non-enzymatic molecules with antioxidant function. MDPI. 10, 579.

Janbandhu, V., Tallapragada, V., Patrick, R., Li, Y., Abeygunawardena, D., Humphreys, D.T., Martin, E.M.M.A., Ward, A.O., Contreras, O., Farbehi, N., 2022. Hif-1a suppresses ROS-induced proliferation of cardiac fibroblasts following myocardial infarction. Cell Stem Cell 29 (2), 281–297.

Keshani, M., Alikiaii, B., Babaei, Z., Askari, G., Heidari, Z., Sharma, M., Bagherniya, M., 2024. The effects of L-carnitine supplementation on inflammation, oxidative stress, and clinical outcomes in critically Ill patients with sepsis: a randomized, double-blind, controlled trial. Nutr. J. 23 (1), 31.

Kumar, S., Gupta, E., Kaushik, S., Kumar Srivastava, V., Mehta, S., Jyoti, A., 2018. Evaluation of oxidative stress and antioxidant status: correlation with the severity of sepsis. Scand. J. Immunol. 87 (4), e12653.

Lakshmi, S.V., Padmaja, G., Kuppusamy, P., Kutala, V.K., 2009. Oxidative stress in cardiovascular disease. Indian J. Biochem. Biophys. 46 (6), 421–440.

Li, X., Guo, W., Xu, R., Song, Z., Ni, T., 2022. The interaction mechanism between gold nanoparticles and proteins: Lysozyme, trypsin, pepsin, γ-globulin, and hemoglobin. Spectrochim. Acta A Mol. Biomol. Spectrosc. 272, 120983.

Li, J., Li, Q., Gao, N., Wang, Z., Li, F., Li, J., Shan, A., 2021. Exopolysaccharides produced by Lactobacillus rhamnosus GG alleviate hydrogen peroxide-induced intestinal oxidative damage and apoptosis through the Keap1/Nrf2 and Bax/Bcl-2 pathways in vitro. Food Funct. 12 (20), 9632–9641.

Lin, C.-P., F.-Y. Lin, P.-H. Huang, Y.-L. Chen, W.-C. Chen, H.-Y. Chen, Y.-C. Huang, W.-L. Liao, H.-C. Huang and P.-L. Liu (2013). "Endothelial progenitor cell dysfunction in cardiovascular diseases: role of reactive oxygen species and inflammation." BioMed Research International **2013**.

Liu, Q., Kim, Y.J., Im, G.B., Zhu, J., Wu, Y., Liu, Y., Bhang, S.H., 2021. Inorganic nanoparticles applied as functional therapeutics. Adv. Funct. Mater. 31 (12), 2008171.

Maity, S., Chakraborty, S., Chakraborti, A.S., 2017. Critical insight into the interaction of naringenin with human haemoglobin: A combined spectroscopic and computational modeling approaches. J. Mol. Struct. 1129, 256–262.

Mandal, G., Bhattacharya, S., Ganguly, T., 2009. Investigations to reveal the nature of interactions between bovine hemoglobin and semiconductor zinc oxide nanoparticles by using various optical techniques. Chem. Phys. Lett. 478 (4–6), 271–276.

Mantzarlis, K., Tsolaki, V., Zakynthinos, E., 2017. Role of oxidative stress and mitochondrial dysfunction in sepsis and potential therapies. Oxid. Med. Cell. Longev. 2017 (1), 5985209.

Matés, J.M., Pérez-Gómez, C., De Castro, I.N., 1999. Antioxidant enzymes and human diseases. Clin. Biochem. 32 (8), 595–603.

Nedić, O., Penezić, A., Minić, S., Radomirović, M., Nikolić, M., Ćirković Veličković, T., Gligorijević, N., 2023. Food Antioxidants and Their Interaction with Human Proteins. Antioxidants 12 (4), 815.

Olajide, P.A., Omowumi, O.S., Odine, G.O., 2022. Pathogenesis of Reactive Oxygen Species: A Review. World News of Natural Sciences 44, 150–164.

Pant, A., Mackraj, I., Govender, T., 2021. Advances in sepsis diagnosis and management: a paradigm shift towards nanotechnology. J. Biomed. Sci. 28, 1–30.

Perez-Araluce, M., Jüngst, T., Sanmartin, C., Prosper, F., Plano, D., Mazo, M.M., 2024. Biomaterials-based antioxidant strategies for the treatment of oxidative stress diseases. Biomimetics 9 (1), 23.

Platanić Arizanović, L., Gligorijević, N., Cvijetić, I., Mijatović, A., Ristivojević, M.K., Minić, S., Kokić, A.N., Miljević, Č., Nikolić, M., 2023. Human Hemoglobin and Antipsychotics Clozapine, Ziprasidone and Sertindole: Friends or Foes? Int. J. Mol. Sci. 24 (10), 8921.

Polsongkram, D., Chamninok, P., Pukird, S., Chow, L., Lupan, O., Chai, G., Khallaf, H., Park, S., Schulte, A., 2008. Effect of synthesis conditions on the growth of ZnO nanorods via hydrothermal method. Phys. B Condens. Matter 403 (19–20), 3713–3717.

Roudbaneh, S.Z.K., Kahbasi, S., Sohrabi, M.J., Hasan, A., Salihi, A., Mirzaie, A., Niyazmand, A., Nanakali, N.M.Q., Shekha, M.S., Aziz, F.M., 2019. Albumin binding, antioxidant and antibacterial effects of cerium oxide nanoparticles. J. Mol. Liq. 296, 111839.

Shahabadi, N., Zendehcheshm, S., Mahdavi, M., 2023. Exploring the In-Vitro Antibacterial Activity and Protein (Human Serum Albumin, Human Hemoglobin and Lysozyme) Interaction of Hexagonal Silver Nanoparticle Obtained from Wood Extract of Wild Cherry Shrub. ChemistrySelect 8 (1), e202204672.

Shaik, M.R., Syed, R., Adil, S.F., Kuniyil, M., Khan, M., Alqahtani, M.S., Shaik, J.P., Siddiqui, M.R.H., Al-Warthan, A., Sharaf, M.A.F., 2021. Mn_3O_4 nanoparticles: Synthesis, characterization and their antimicrobial and anticancer activity against A549 and MCF-7 cell lines. Saudi Journal of Biological Sciences 28 (2), 1196–1202.

Shaito, A., K. Aramouni, R. Assaf, A. Parenti, A. Orekhov, A. El Yazbi, G. Pintus and A. H. Eid (2022). "Oxidative stress-induced endothelial dysfunction in cardiovascular diseases.".

Singh, N., Savanur, M.A., Srivastava, S., D'Silva, P., Mugesh, G., 2017. A redox modulatory Mn_3O_4 nanozyme with multi-enzyme activity provides efficient cytoprotection to human cells in a Parkinson's disease model. Angew. Chem. 129 (45), 14455–14459.

Singh, N., Savanur, M.A., Srivastava, S., D'Silva, P., Mugesh, G., 2019. A manganese oxide nanozyme prevents the oxidative damage of biomolecules without affecting the endogenous antioxidant system. Nanoscale 11 (9), 3855–3863.

Takano, H., Zou, Y., Hasegawa, H., Akazawa, H., Nagai, T., Komuro, I., 2003. Oxidative stress-induced signal transduction pathways in cardiac myocytes: involvement of ROS in heart diseases. Antioxid. Redox Signal. 5 (6), 789–794.

van de Weert, M., 2010. Fluorescence quenching to study protein-ligand binding: common errors. J. Fluoresc. 20, 625–629.

Vázquez-Olmos, A., Redón, R., Rodríguez-Gattorno, G., Mata-Zamora, M.E., Morales-Leal, F., Fernández-Osorio, A.L., Saniger, J.M., 2005. One-step synthesis of Mn_3O_4 nanoparticles: Structural and magnetic study. J. Colloid Interface Sci. 291 (1), 175–180.

Wang, Y., Hou, C., Lin, X., Jiang, H., Zhang, C., Liu, G., 2021. Dye degradation studies of hausmannite manganese oxide (Mn_3O_4) nanoparticles synthesized by chemical method. Appl. Phys. A 127, 1–7.

Wang, F., Liang, Q., Ma, Y., Sun, M., Li, T., Lin, L., Sun, Z., Duan, J., 2022b. Silica nanoparticles induce pyroptosis and cardiac hypertrophy via ROS/NLRP3/Caspase-1 pathway. Free Radic. Biol. Med. 182, 171–181.

Wang, D., Wang, C., Liang, Z., Lei, W., Deng, C., Liu, X., Jiang, S., Zhu, Y., Zhang, S., Yang, W., 2022a. Protection of zero-valent iron nanoparticles against sepsis and septic heart failure. J. Nanobiotechnol. 20 (1), 405.

Ware, W.R., 1962. Oxygen quenching of fluorescence in solution: an experimental study of the diffusion process. J. Phys. Chem. 66 (3), 455–458.
Xiao, L., Chen, Y., 2020. Ulinastatin-gold nanoparticles reduce sepsis-induced cardiomyocyte apoptosis through NF-κB pathway inactivation. Nanosci. Nanotechnol. Lett. 12 (12), 1399–1405.
Xing, S., Zhou, Z., Ma, Z., Wu, Y., 2011. Facile synthesis and electrochemical properties of Mn_3O_4 nanoparticles with a large surface area. Mater. Lett. 65 (3), 517–519.
Yang, Y.T., Si, P.Z., Choi, C.J., Ge, H.L., 2019. Large coercivity and exchange bias in Mn_3O_4 nanoparticles prepared by laser ablation method. J. Magn. Magn. Mater. 489, 165481.
Yang, X., Zhao, L., Zheng, L., Xu, M., Cai, X., 2018. Polyglycerol grafting and RGD peptide conjugation on MnO nanoclusters for enhanced colloidal stability, selective cellular uptake and cytotoxicity. Colloids Surf. B Biointerfaces 163, 167–174.
Yewale, M.A., Jadhavar, A.A., Kadam, R.A., Velhal, N.B., Nakate, U.T., Teli, A.M., Shin, J.C., Nguyen, L.N., Shin, D.K., Kaushik, N.K., 2022. Hydrothermal synthesis of manganese oxide (Mn_3O_4) with granule-like morphology for supercapacitor application. Ceram. Int. 48 (19), 29429–29437.
Yoon, C.S., Kim, H.K., Mishchenko, N.P., Vasileva, E.A., Fedoreyev, S.A., Shestak, O.P., Balaneva, N.N., Novikov, V.L., Stonik, V.A., Han, J., 2019. The protective effects of echinochrome A structural analogs against oxidative stress and doxorubicin in AC16 cardiomyocytes. Mol. Cell. Toxicol. 15, 407–414.
Zeinabad, H.A., Kachooei, E., Saboury, A.A., Kostova, I., Attar, F., Vaezzadeh, M., Falahati, M., 2016. Thermodynamic and conformational changes of protein toward interaction with nanoparticles: a spectroscopic overview. RSC Adv. 6 (107), 105903–105919.
Zhang, L., Y. Liu, J. Y. Li, L. Z. Li, Y. L. Zhang, H. Y. Gong and Y. Cui (2018). "Protective effect of rosamultin against H_2O_2-induced oxidative stress and apoptosis in H9c2 cardiomyocytes." Oxidative Medicine and Cellular Longevity **2018**.
Zhang, W., Yuan, S.L., Qiang, J.C., Huang, H., Da, L., Ying, S., Zhang, H.G., 2024. Malvidin Mitigates Sepsis-induced Cardiac Injury by Modulating the TLR4-iNOS-COX-2 Inflammatory Pathway and the Bax/Bcl-2/Cyto-C Mitochondrial Apoptosis Pathway in a p38 MAPK-dependent Manner. Biomed. Environ. Sci. 37 (2), 221–227.
Zolghadri, S., Saboury, A., Golestani, A., Divsalar, A., Rezaei-Zarchi, S., Moosavi-Movahedi, A., 2009. Interaction between silver nanoparticle and bovine hemoglobin at different temperatures. J. Nanopart. Res. 11, 1751–1758.
Zolghadri, S., Saboury, A., Amin, E., Moosavi-Movahedi, A., 2010. A spectroscopic study on the interaction between ferric oxide nanoparticles and human hemoglobin. J. Iran. Chem. Soc. 7, S145–S153.